ACS APPLIED MATERIALS & INTERFACES

Research Article

www.acsami.org

Multilayered Magnetic Gelatin Membrane Scaffolds

Sangram K. Samal,[†,‡,§] Vitaly Goranov,[†] Mamoni Dash,[∥] Alessandro Russo,[⊥] Tatiana Shelyakova,[⊥] Patrizio Graziosi,[†] Lisa Lungaro,[†,#] Alberto Riminucci,[†] Marc Uhlarz,[▽] Manuel Bañobre-López,[○] Jose Rivas,[◆] Thomas Herrmannsdörfer,[▽] Jayakumar Rajadas,[¶] Stefaan De Smedt,[§] Kevin Braeckmans,[§] David L. Kaplan,[*,‡] and V. Alek Dediu[*,†]

[†]Spintronic Devices Division, Institute for Nanostructured Materials ISMN-CNR, Via Gobetti 101, 40129 Bologna, Italy

[‡]Department of Biomedical Engineering, Tufts University, 4 Colby Street, Medford, Massachusetts 02155, United States

[§]Laboratory of General Biochemistry and Physical Pharmacy, Ghent University, Ottergemsesteenweg 460, B-9000 Ghent, Belgium

[∥]Polymer Chemistry & Biomaterials Research Group, Ghent University, Krijgslaan 281, S4-Bis, B-9000 Ghent, Belgium

[⊥]Laboratory of Biomechanics and Technology Innovation, NABI, Rizzoli Orthopaedic Institute, Via di Barbiano 1/10, 40136 Bologna, Italy

[#]Osteoarticular Research Group, Centre for Genomic and Experimental Medicine, The University of Edinburgh, Western General Hospital, Crewe Road, Edinburgh EH4 2XU, United Kingdom

[▽]Dresden High Magnetic Field Laboratory (HLD-EMFL), Helmholtz-Zentrum Dresden-Rossendorf, Bautzner Landstrasse 400, 01328 Dresden, Germany

[○]International Iberian Nanotechnology Laboratory (INL), Av. Mestre José Veiga, 4715-330 Braga, Portugal

[◆]Department of Applied Physics, Faculty of Physics, Universidade de Santiago de Compostela, 15782 Santiago de Compostela, Spain

[¶]Biomaterials and Advanced Drug Delivery Laboratory, Cardiovascular Pharmacology Division, Stanford Cardiovascular Institute, Stanford University, 1050 Arastradero, Palo Alto, California 94304, United States

ABSTRACT: A versatile approach for the design and fabrication of multilayer magnetic scaffolds with tunable magnetic gradients is described. Multilayer magnetic gelatin membrane scaffolds with intrinsic magnetic gradients were designed to encapsulate magnetized bioagents under an externally applied magnetic field for use in magnetic-field-assisted tissue engineering. The temperature of the individual membranes increased up to 43.7 °C under an applied oscillating magnetic field for 70 s by magnetic hyperthermia, enabling the possibility of inducing a thermal gradient inside the final 3D multilayer magnetic scaffolds. On the basis of finite element method simulations, magnetic gelatin membranes with different concentrations of magnetic nanoparticles were assembled into 3D multilayered scaffolds. A magnetic-gradient-controlled distribution of magnetically labeled stem cells was demonstrated in vitro. This magnetic biomaterial−magnetic cell strategy can be expanded to a number of different magnetic biomaterials for various tissue engineering applications.

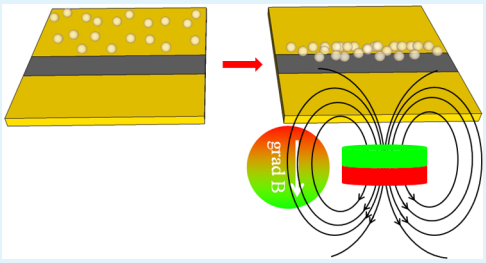

KEYWORDS: *magnetic, nanoparticles, gelatin, scaffold, biomaterials, gradient, tissue engineering*

1. INTRODUCTION

Recent advances in designing biomaterial scaffolds are at the forefront of the development of tissue engineering and hold promise for various therapeutic applications.[1−4] Polymeric scaffolds combined with biomolecules and stem cells have accelerated the regeneration of tissue defects.[5,6] As a result, considerable effort has been dedicated toward the development of manufacturing technologies for the production of customized biomaterials with reproducible internal morphology, to support the transport of bioagents and improve tissue regeneration outcomes in vitro and in vivo. However, there is a dearth of delivery strategies for localization of such material systems to target sites, short of injection or surgical implantation. Thus, new concepts toward targeted delivery would be instructive for the field of tissue engineering and potentially offer important new applications. Thus, scaffolds with internal magnetic gradients were explored here as a way to overcome existing localization challenges.[7,8] Recently, several advanced technologies were reported in the development of magnetic nanoparticles (MNPs) in various diagnostic and therapeutic applications. These systems have triggered the development of novel three-dimensional (3D) magnetic-gradient scaffolds that play an important role in the cell signaling that guide the migration, proliferation, and differentiation of cells.[9−12] MNPs have been widely used in biomedical applications due to their biocompatibility, large

Received: July 27, 2015
Accepted: September 29, 2015
Published: October 9, 2015

DOI: 10.1021/acsami.5b06813
ACS Appl. Mater. Interfaces 2015, 7, 23098−23109

surface functionalization feasibility, tunable physicochemical properties, and ability to interact with an externally applied magnetic field.[13,14] In particular, colloidally stable iron oxide MNPs (SPIONs) are among the most biocompatible magnetic nanoparticles used in the biomedical field, additionally featuring low-cost synthesis with high scale-up potential.[15] Several SPIONs-based aqueous dispersions have already reached the market for biomedical use or are in late-phase clinical trials. NanoTherm or Resovist are colloidal stable SPIONs used as small nanoheaters in magnetic hyperthermia and magnetic resonance imaging (MRI) as enhanced T_2-contrast agents in cells of the mononuclear phagocyte system (MPS), respectively. The development of magnetic nanoparticles (MNPs) in theranostic applications has exploited the unique tunable physicochemical properties of MNPs and their ability to be externally manipulated via magnetic fields. The incorporation of MNPs in polymeric networks provides magnetic responsive properties. On the basis of this, recently, the concept of scaffolds with internal magnetic gradients has been introduced to overcome some localization challenges.[4,16]

The working principle of magnetic scaffolds is based on the formation of a nonuniform magnetization within the scaffold by methods that do not impair the biocompatibility or other important functions. The spatial variation of magnetization generates magnetic field gradients, causing forced movement of magnetic objects, even inside the scaffold. By attaching selected bioagents to the MNPs, the magnetic scaffolds provide targeted biodelivery inside the scaffolds. The scaffolds should have a small coercive field so that magnetization as well as local intrascaffold magnetic gradients is activated when a homogeneous external magnetic field is applied. The realization of scaffolds with magnetic gradients represents a conceptually novel technological challenge.[17−19] Among various strategies to design magnetic biomaterials, the incorporation of MNPs into polymeric solutions followed by cross-linking or infusion methods is most widely used.[7,8,20−22] The incorporation of MNPs is expected to improve scaffold bioactivity.[23−27] The external applied magnetic field could induce torque magnetic forces into the scaffold that offers mechanical stimulation to the cells, therefore favoring their proliferation and differentiation.[28,29] Under a magnetic field, these scaffolds can be induced to undergo physical changes such as elongation, contraction, or bending.[30−32] These magnetic-sensitive biomaterials are useful in comparison to other stimuli-responsive biomaterials because magnetic stimulation acts at a distance (noncontact force) that is noninvasive and convenient to adapt for therapeutic devices.[33−36] The magnetic properties of multilayered membrane scaffolds can be utilized to construct biomaterials for site-specific and/or time-controlled delivery, magnetic resonance imaging contrast agents, sensors, and artificial muscles.[7,37−42] This approach also includes various separation membranes and hyperthermia treatments under external magnetic stimuli.[43−46]

The choice of materials for effective cell development is important for tissue engineering. Gelatin is a biocompatible material obtained from collagen by partial hydrolysis and denaturation, during which the triple helix structure is broken down to form random gelatin protein coils. Gelatin has shown excellent features for the design of cell-compatible and degradable biomaterials with support of cellular bioactivity.[47−51] The U.S. Food and Drug Administration (FDA) classified gelatin as a safe excipient, which is currently used as a constituent of various biomaterials for biomedical applications.[52] The gelatin protein networks are composed of hydrophobic and hydrophilic moieties, with hydrophilic functional groups (−OH, −COOH, $-NH_2$, $-CONH_2$) able to chelate metal ions.

In the present article, multilayered magnetic gelatin scaffolds were developed that generate magnetic field gradients upon the application of an external magnetic field. Thus, this system provides desirable biomaterial features for optimizing loading, proliferation, and differentiation of cells. The strategy was to combine the magnetic behavior of SPIONs along with gelatin protein network for the fabrication of a magnetic scaffold with high saturation magnetization and magnetic gradient along its longitudinal axis. Different assemblies of magnetic gelatin sheets with different concentrations of SPIONs into multilayered magnetic gelatin scaffolds were characterized by a tunable and variable magnetic gradient that can point in different directions and is activated by an external uniform magnetic field. The shape and strength of the magnetic gradients realized inside the scaffolds were modeled by use of the COMSOL finite element analysis package. The characteristics of these magnetic scaffolds were evaluated by investigating magnetic properties and thermal responses to a remotely applied external magnetic field. The biocompatibility of the magnetic scaffolds was evaluated with human mesenchymal stem cells (hMSCs). The present work is aimed at designing magnetic scaffolds via a simple strategy and understanding the effect of their magnetic gradient on cellular responses in vitro.

2. EXPERIMENTAL SECTION

2.1. Materials. Gelatin from bovine skin Type B, powder, BioReagent, suitable for cell culture was purchased from Sigma-Aldrich (G9391, Sigma-Aldrich, Italy) with gel strength ∼225 g Bloom. Water-dispersed poly(acrylic acid) (PAA)-coated magnetic nanoparticles (FF-PAA) were synthesized by alkaline coprecipitaion of iron(II) and iron(III) salts in aqueous solution as reported previously.[53] The average particle size (by transmission electron microscopy) and distribution was 9 ± 2 nm (85% of the total amount of particles), and they were pseudospherical in shape and highly crystalline, as deduced from the X-ray diffraction data (not shown).

2.2. Zeta Potential Measurements of Gelatin−MNPs Solutions. Dynamic light scattering (DLS), a noninvasive technique, was employed to characterize the surface charge of the MNPs and gelatin−MNPs by measuring the zeta potential using a Zetasizer Nano Series (Malvern Instruments, Hoeilaart, Belgium). The gelatin−MNPs suspensions were added into the disposable folded capillary cells (DTS 1070), and the measurements were performed at 45 °C. The histograms were split for figure clarity.

2.3. Preparation of Magnetic Gelatin Layers. Gelatin solution was prepared by suspending 10 wt % of dried gelatin in slightly hot deionized water, and the suspension was subsequently dissolved under agitation for 3 h under a nitrogen blanket at 40 °C to force the gelatin into a clear transparent solution.

Then, the gelatin solution was mixed with different concentrations of FF-PAA (Table 1) and refluxed together under a nitrogen blanket with stirring for 1 h at 40 °C to form a homogeneous gelatin/FF-PAA binary blend solution. Then, the solution was sonicated for 10 min at 37 °C to eliminate air bubbles. The solutions obtained were then cast into multilayer membranes in polystyrene plates, dried in air at room temperature for 48 h, and subsequently desicated in order to ensure complete removal of remaining water. The polystyrene plate was kept level during the drying process to obtain even membrane thickness, and the membranes were subsequently cross-linked via carbodimide chemistry.[54−57]

2.4. Atomic Force Microsopy Analysis. AFM measurements were performed on a Nanoscope III/Multimode instrument by Digital Instruments, operating in tapping mode with Etalon probes by NT-MDT, at a resonance frequency of about ∼230 kHz. The cantilever

DOI: 10.1021/acsami.5b06813
ACS Appl. Mater. Interfaces 2015, 7, 23098−23109

Table 1. Sample Abbreviation and Different Ratios of Gelatin-B (10% w/v) and Magnetic Nanoparticles

sample	gelatin-B (μL)	magnetic nanoparticles (% w/v)	saturation magnetization (emu/g)
blank	1500	0	0.0
A	1475	1.7	0.3
B	1450	3.4	0.6
C	1400	6.7	0.8
D	1250	16.7	2.6
E	1000	33.4	6.1
F	750	50	10.1
G	500	66.7	16.1
H	250	83.4	38.7

phase was set at zero and controlled automatically by the software in order to measure the phase shift reliably.

2.5. Thermogravimetric Analysis (TGA). TGA experiments were performed with a TA Instruments Q500 thermo-balance (TA Instruments, Milan, Italy) with thermogravimetric analyzer software (Universal Analysis 2000). Sample weights were between 4 and 6 mg and were scanned at 10 °C·min^{-1}. The temperature range was 30 to 800 °C under a 60 mL·min^{-1} flow rate of nitrogen.[46]

2.6. Differential Scanning Calorimetry (DSC). DSC of the samples were assessed on a Mettler DSC822e module (Mettler Toledo, Milan, Italy) controlled by STARe software under a nitrogen atmosphere at an 80 mL·min^{-1} flow rate with three scans. Samples of 3−5 mg were weighed in standard 40 μL aluminum pans, and an empty pan was used as reference. Measurements were performed in accordance with ASTM D3418 methods under a nitrogen flow rate of 80 mL·min^{-1} according to the following protocols: (a) First heating scan from −20 to 220 °C at 10 °C·min^{-1} and 3 min of isothermal conditions at the end; (b) first cooling scan from 220 to −50 °C at −10 °C·min^{-1} and 3 min of isothermal conditions at the end; and (c) second heating scan from −50 to 300 °C at 10 °C·min^{-1}.

2.7. Attenuated Total Reflectance FTIR (ATR-FTIR). The interaction of MNPs with gelatin's amino acids was evaluated by ATR-FTIR analysis. The experiment was performed on gelatin and magnetized gelatin membrane samples with a JASCO FTIR-6200 (Tokyo, Japan) equipped with a MIRacle attenuated total reflection (ATR) Crystal Ge (IR penetration, 0.66 mm) cell in reflection mode, and absorbance spectra were collected at 32 scans coded with 4 cm^{-1} resolution in the region 4000−550 cm^{-1}. The spectra were split into two parts, 4000−2600 and 1900−550 cm^{-1}, in order to zoom in on the peaks.

2.8. Magnetization Measurements. Magnetization measurements were performed using a superconducting quantum interference device (SQUID) magnetometer (Quantum Design Inc., San Diego, CA, USA). This instrument measures the total magnetic moment of a sample, including all atomic and molecular magnetic contributions. The magnetization of the sample was calculated as the ratio between magnetic moment and sample mass. A microbalance (Sartorius model M3P) was used to determine sample masses. Each sample was fixed to a custom-made sample holder that ensures a canceling of magnetic background contributions. The magnetic field was either swept at 37 °C or was held constant during a temperature sweep. Having reached predetermined values for field and temperature, the samples were consistently moved through a pick-up coil system connected to the SQUID via a flux transformer. The movement of the sample effects a magnetic flux change in the superconducting pick-up circuit, which is sensed and amplified by a SQUID sensor and its feedback control circuit. The SQUID output signal is directly proportional to the sample's magnetic moment. Knowing the samples' geometries, the samples' demagnetization factors were calculated to determine the quantitatively correct internal magnetic field values. The results showed that the demagnetization contributions were well below 1% of the measured magnetizations and can thus be neglected. In the present study, the pure gelatin layer magnetization at T = 310 K and at any magnetic field is smaller than 0.1 emu/g and is thus negligible.

2.9. Magnetic-Hyperthermia Measurement. The gelatin membranes containing different concentrations of MNPs were attached to an optical fiber (temperature probe) that was then located in the midpoint of a water-cooled copper coil, where the magnitude of the oscillating magnetic field generated by an AC current circulating through it was maximal. High vacuum (∼10^{-7} bar) was applied in the chamber between the sample and the electronics to avoid any extrinsic heating contribution. The experimental values of frequency and intensity of this alternating magnetic field used in the experiments were 293 kHz and 30 mT, respectively. Then, the temperature increase was recorded as a function of time during the experiment. The main advantage of magnetic hyperthermia is that we can remotely control the activation of the MNPs embedded in the scaffold, so the MNPs behave as small nanoheaters, increasing the local temperature and inducing thermal stimuli to the surrounding tissues, which can be used to selectively kill harmful cells (i.e., tumor cells) or to trigger the release of a growth factor for tissue regeneration. Additionally, the external applied magnetic field could induce torque magnetic forces into the scaffold that would presumably be translated into mechanical stimulation to the cells, therefore favoring their proliferation and differentiation.[28,29]

2.10. Magnetization of Cells. Human mesenchymal stem cells (hMSCs) were seeded in T75 flasks at a concentration of 3.5 × 10^3/cm^2 using Alpha MEM growth medium, (M0644, Sigma-Aldrich) supplemented with 10% of fetal bovine serum (F9665, Sigma-Aldrich), 1% HEPES (4-(2-hydroxyethyl)piperazine-1-ethanesulfonic acid, *N*-(2-hydroxyethyl)piperazine-*N*′-(2-ethanesulfonic acid) (H3784, Sigma-Aldrich), 1% sodium pyruvate, and 1% antibiotic solution.[58] The cells were left to adhere to bottom of the flask at 37 °C in 5% CO_2. To make the cells sensitive to the magnetic field, when the cells adhered, 14 μL of FF-PAA was added to the culture medium. The cells were incubated overnight. After 24 h, the medium was changed and replaced with fresh medium. When the cells reached confluence, they were trypsinized, centrifuged at 1000 rpm for 5 min, and used for further experiments. The magnetization level was set approximately to 100 pg of MNPs per cell, a concentration that allowed cells to be magnetically manipulated by permanent laboratory magnets.

2.11. Cytotoxicity Analysis. The cytotoxic effects of magnetic gelatin membranes were studied by measuring cell viability 2 days after seeding. For this purpose, hMSCs were seeded onto each sample was seeded. The quantification of viable cells was performed using a (3-(4,5-dimethylthiazol-2-yl)-2,5-diphenyltetrazolium bromide (MTT) test. This colorimetric bioassay tracks the reduction of the yellow tetrazolium salt (MTT) to a purple/blue formazan by the metabolic activity of the cells.[59] Each sample was seeded with 40 000 hMSCs under standard cell culture conditions. Cell viability was determined using a live/dead viability kit (L-3224, Molecular Probes, ThermoFisher). Visualization of cells attached to the membrane scaffold was determined by staining with calcein AM and ethidium homodimer-1. Green fluorescence by calcein reacting with an intracellular esterase indicates live cells, whereas red fluorescence indicated by ethidium homodimer denotes dead cells.

2.12. Cell Manipulation and Localization under an External Magnetic Field. The viability of magnetized hMSCs after cell manipulation by 1.2 T magnetic fields was performed using three different concentrations of MNPs, 50, 100, and 200 pg/hMSc, and compared with the blank, hMSc without any MNPs. In order to estimate the ability of magnetic scaffolds to manipulate cells and their localization, cell motility was assessed in a specially designed set up developed in-plane under horizontal magnetic field gradients. This system is compatible with direct microscopy under standard cell culture conditions. Magnetically labeled hMSCs resuspended in growth medium were added to a Petri dish with an 80 μm thick and 20 mm wide membrane scaffold composed of a 3 mm magnetic strip (membrane type C) and a nonmagnetic (blank membrane) residual part. Cell motility was investigated starting from the moment that a permanent magnet (8 cm diameter and 1.2 T residual magnetization) was rapidly set at a 15 mm distance from the magnetic strip, from the side opposite that of the cells.

DOI: 10.1021/acsami.5b06813
ACS Appl. Mater. Interfaces 2015, 7, 23098−23109

2.13. Statistical Analysis. Statistical analysis was performed by one-way ANOVA posthoc *t*-tests, $p < 0.05$, with Bonferroni correction using standard statistical analysis software (Excel statistics, Microsoft, USA)

3. RESULTS AND DISCUSSION

3.1. Zeta Potential Measurement of Gelatin−MNPs Solution. Zeta potential measurements of gelatin−MNPs solutions are depicted in Figure 1. The results indicated that the gelatin solution and MNPs showed slightly positive and highly negative zeta potentials, respectively.

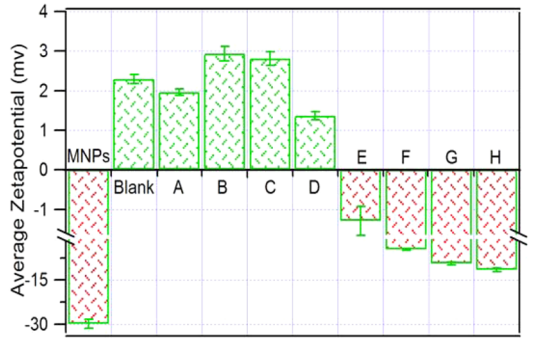

Figure 1. Zeta potential measurements of gelatin−MNPs solutions at different concentrations of MNPs at 45 °C.

The addition of MNPs into the gelatin solution initiated interactions between the carboxyl and amine group of the amino acids present in gelatin and the metallic MNPs. The addition of a low concentration of MNPs initially decreased the positive charge of the gelatin solution, whereas further increasing the MNPs concentration increased the positive charge of the solution. Furthermore, increasing the concentration of MNPs in the gelatin−MNPs solutions increased the negative charge. However, at higher concentrations of MNPs, the charge of the gelatin−MNPs solution increased up to −11.5 mV, which was lower compared to the initial charge of the pristine MNPs (−29.7 mV). It is hypothesized that the initiation of interactions between the different functional groups upon addition of MNPs into the gelatin solution reduced the surface charge.

3.2. Fabrication of 3D Multilayered Magnetic Gelatin Scaffolds. A schematic representation of the fabrication of the 3D multilayered magnetic gelatin scaffolds is shown in Figure 2A. The polymeric magnetic nanocomposite material is based on the combination of biocompatible biopolymer gelatin and different ratios (Figure 2B) of superparamagnetic Fe_3O_4 nanoparticles (Table 1). The MNPs' surface interacts with the free amino functional groups present in gelatin's chemical structure, improving the colloidal stability and homogeniety of the magnetic dispersion. In addition, MNPs are expected to chelate free amino and carboxylic groups on the amino acids of gelatin and are randomly dispersed in a gelatin solution. The homogeneous mixing of the MNPs in gelatin is a prerequisite for further engineering multilayered magnetic gelatin membrane scaffolds. These gelatin solutions containing homogeneously distributed MNPs were finally cast into 39 mm diameter and 20 μm thick discs (Figure 2B). The scaffold material is completed upon subsequent cross-linking of the carboxylic acid and amine groups of gelatin with *N*-(3-(dimethylamino)propyl)-*N*′-ethylcarbodiimide hydrochloride (EDC) and *N*-hydroxysuccinimide (NHS).

3.3. Atomic Force Microscopy Analysis. Membranes were analyzed by atomic force microscopy (AFM) in tapping mode.[60] The top row of Figure 3 shows the AFM topography of the membranes, and the bottom row shows the corresponding phase-contrast images. The concentration of MNPs increases from left to right in each column (blank, D, H). The first observation is that the surface roughness increased with increasing MNP concentration, from 6 nm for the blank sample (no MNPs) to 40 nm for sample H. The surface of blank gelatin membrane scaffolds with no MNPs appears to be homogeneous, and its morphological features do not correlate with the phase-contrast image, which is expected for a material consisting of a single component. Sample D, with a lower concentration of MNPs, showed clear differences in the material between harder (bright green) and softer (dark green to blue) regions (Figure 3D, bottom row). Surprisingly, in sample H, with a higher concentration of MNPs, the distribution of material at the surface appears to be as homogeneous as that in the blank sample (Figure 3H, bottom row).

The surface was further quantitatively analyzed by scaling the root-mean-square (rms) roughness R_{rms}. This quantity increases as the scanned area increase until it plateaus above a threshold area.[61] Thus, the study of R_{rms} versus area is considered to be an excellent tool to determine statistically the correlation lengths that characterize the surface. The image size at which R_{rms} saturates is a characteristic length and represents the size above

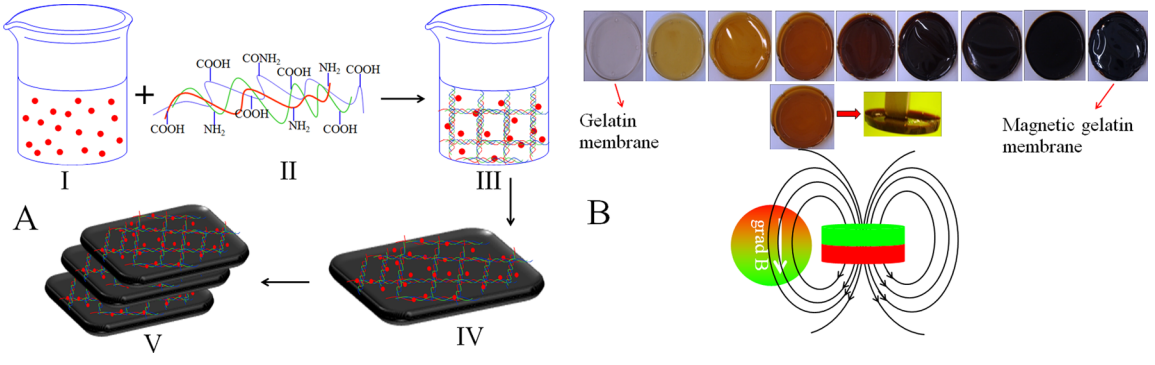

Figure 2. (A) Fabrication of a multilayered magnetic gelatin scaffold: I, superparamagnetic MNPs; II, biocompatible polymer gelatin; III, gelatin−MNPs suspension; IV, magnetic membrane monolayer; and V, multilayered magnetic scaffold. (B) Magnetic gelatin membranes with increasing MNPs concentration from left to right as well as a representation of the properties of the magnetic gradient.

DOI: 10.1021/acsami.5b06813
ACS Appl. Mater. Interfaces 2015, 7, 23098−23109

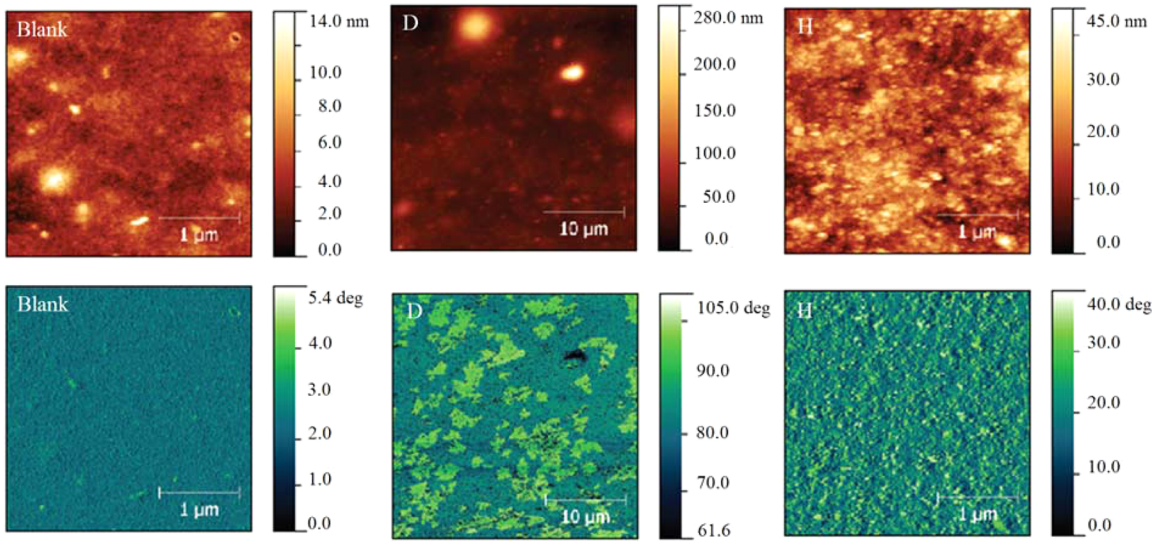

Figure 3. Topographies (top row) and corresponding phase-contrast (bottom row) images of the membranes with different MNPs concentrations (blank and samples D and H).

which the surface features appear to be indistinguishable. This characteristic length in the phase-contrast images of the membranes decreased as the MNPs concentration increased, from 50 μm for sample B (data not shown) to 3 μm for sample H (with the highest MNP content). This confirms quantitatively that, from a material composition perspective, the membranes with the highest MNPs content are more homogeneous than those with low MNPs content, although they are rougher topographically. Although this aspect of the materials requires further investigation, it is clear that MNP aggregation is different for intermediate and high MNPs concentrations than it is at low concentrations. We tentatively ascribe the higher homogeneity at high MNP concentrations to a greater density of nucleation centers. By comparing the pictures in the top and bottom rows of Figure 3, the phase shift features and MNP distribution do not correlate with the observed morphological features, which indicates complex phase mixing. Higher magnification AFM images for samples D and H (Figure 4) were then obtained. The mean size of the

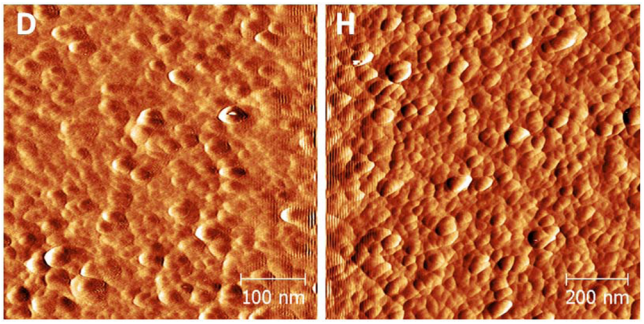

Figure 4. Phase-contrast images and corresponding height−height correlation function for samples D and H.

MNPs on the membrane scaffold's surface was expected to be around 20 nm, indicating the existence of some interactions between the amino acids of gelatin and the MNPs.

3.4. Thermogravimetric Analysis (TGA). The thermal stability of the MNPs encapsulated in gelatin membranes was analyzed by TGA (Figure 5a,b). All traces show continuous weight loss up to 800 °C, with the first step loss in the range 30−120 °C attributed to the loss of moisture, followed by continuous weight loss from 250 °C onward due to the decomposition of the gelatin network at elevated temperatures. The thermal investigation by TGA led to the observation that magnetized membranes showed a two-step degradation pattern, which might be due to some interactions between gelatin and the MNPs. Furthermore, the magnetized membranes possessed higher residue content at 700 °C due to the presence of magnetic nanoparticles compared to that of nonmagnetized gelatin membrane scaffolds. The results suggest the existence of some interactions between gelatin molecules and MNPs, and this is also in agreement with the AFM results.

3.5. Differential Scanning Calorimetry (DSC). The first heating (Figure 6a) curve shows that having a low amount of MNPs infused increased the hydrophilic properties of the membrane scaffolds. With increasing the MNPs concentration in the membrane, the hydrophilic properties decreased compared to those of a pure gelatin membrane scaffold. The results demonstrated that a higher concentration of nanostructured MNPs resulted in more rapid evaporation of water, which is evident from the shift in the spectra. The second heating (Figure 6b) revealed a change in the melting temperature prior to degradation. In addition, MNPs-containing membrane scaffolds showed a phase change in the bending spectra at 220 °C prior to degradation, which supports the hypothesis of there being some interaction between the gelatin network and the MNPs. The spectra of the membrane having a higher content of MNPs shows different behavior, possibly due to the presence of the MNPs, which increased the thermal stability of the magnetic gelatin nanocomposite membranes. The DSC analysis demonstrated the presence of some interactions between the gelatin molecules and the MNPs, which is in agreement with the AFM and TGA results.

3.6. Attenuated Total Reflectance FTIR (ATR-FTIR). ATR-FTIR was used to observe the interactions between gelatin and MNPs in magnetized gelatin membranes (Figure 7). The general characteristic bands of gelatin appear at 1627 cm^{-1} for amide-I, 1542 cm^{-1} for amide-II, and 1232 cm^{-1} for amide-III. All of these characteristic bands are also observed in

DOI: 10.1021/acsami.5b06813
ACS Appl. Mater. Interfaces 2015, 7, 23098−23109

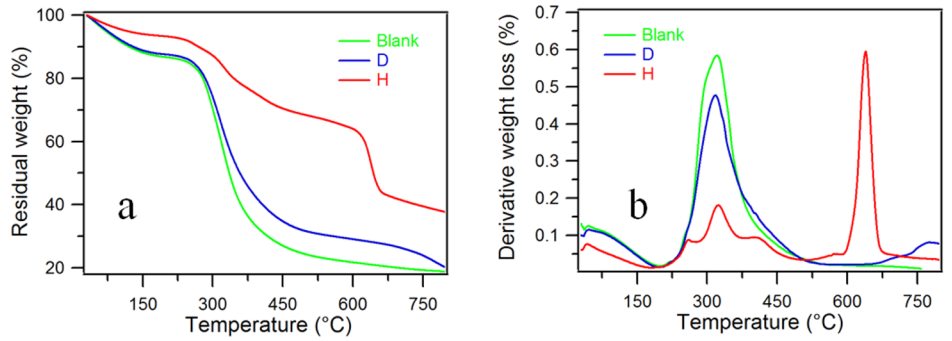

Figure 5. TGA spectra of gelatin (blank) and magnetic gelatin membrane scaffolds (samples D and H): (a) residual weight loss and (b) derivative weight loss at 10 °C·min^{-1} over the temperature range 30−800 °C with a 60 mL·min^{-1} flow rate of nitrogen using a TA Q500 instrument.

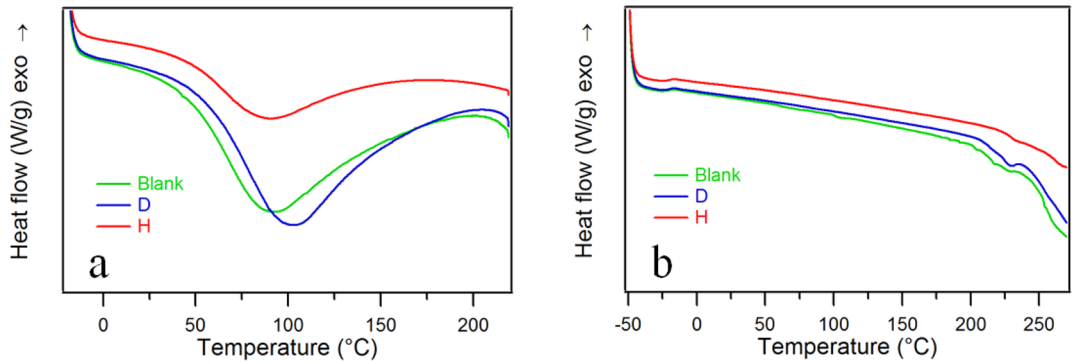

Figure 6. Differential scanning spectra of gelatin (blank) and magnetic gelatin scaffolds (samples D and H): (a) first and (b) second heating spectra at a scan rate of 10 °C·min^{-1} using a Mettler DSC822e module with STARe software under a nitrogen atmosphere at an 80 mL·min^{-1} flow rate.

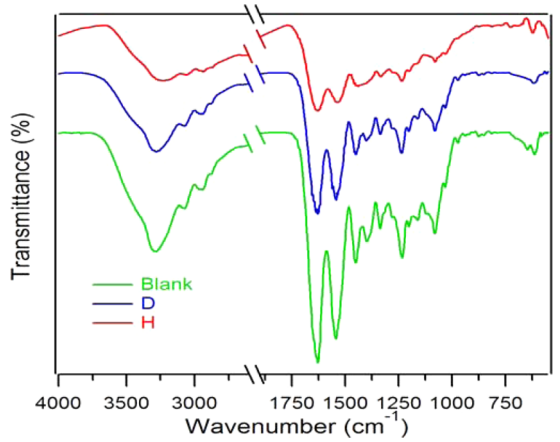

Figure 7. ATR-FTIR spectra of gelatin (blank) and magnetized gelatin membranes (samples D and H).

MNPs-containing gelatin membrane scaffolds, with decreased band intensity and broadening.

3.7. Magnetization Measurements. The magnetic properties of samples with different MNPs concentrations in the gelatin monolayer were measured along with pure gelatin as a reference using a SQUID magnetometer. The magnetization of pure gelatin at T = 310 K was smaller than 0.1 emu/g at all of the magnetic fields used in this study; hence, the contribution of gelatin can be neglected when comparing the magnetic properties of the gelatin membranes containing MNPs. The field-dependent magnetization of the samples was measured at 37 °C (Figure 8). The coercive field was small and comparable in size for all investigated MNP concentrations. The magnetization saturates at field values that are similar for the different MNP concentrations. The saturation magnetization of bulk Fe_3O_4 at room temperature is 96 emu/g, and corresponding values of up to 96 emu/g are obtained for the

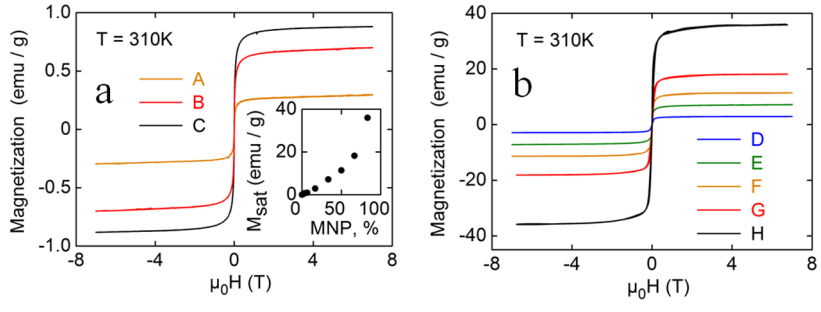

Figure 8. Magnetization at T = 310 K for gelatin membranes containing various MNPs concentrations: (a) low-concentration MNP samples, A−C, and (b) high-concentration MNPs samples, D−H. The inset in panel (a) indicates the saturation magnetization vs MNP concentration.

DOI: 10.1021/acsami.5b06813
ACS Appl. Mater. Interfaces 2015, 7, 23098−23109

best superparamagnetic particles, as reported.[62] The saturation magnetization for sample H with the highest MNP concentration was 36 emu/g.

A nonlinear dependence of the saturation magnetization on the MNPs' concentration was observed (Figure 8). An effective MNP diameter D_m was determined on the basis of the observed saturated magnetization and initial susceptibility, dM/dH (H = 0). The underlying assumption (confirmed by AFM for high-concentration samples) was that the MNPs were monodisperse.[63] The sample with the highest concentration of MNPs gave D_m = 18 nm. This effective diameter is substantially larger than that determined from TEM (9 ± 2 nm). Such discrepancies are presumably caused by small particle aggregates due to interactions between the carboxylic groups coating the magnetic nanoparticles and the chelating amino acids present in gelatin. Even though they improve the colloidal stability of the MNPs in solution, small aggregates can be produced when the sample is gelled as a consequence of the collapse of the structure and the subsequent reduction of the interparticle distance. This is in agreement with the results from the AFM images acquired on the different magnetic nanocomposites and shown in Figure 3. In some cases, the MNP cores are strongly affected by the adsorbed, highly polar molecules, leading to the formation of a nonmagnetic surface shell on the MNPs.[64,65] Thus, only the inner cores of the MNPs might be magnetic.

Figure 9 shows the temperature dependence of the magnetization of a gelatin membrane with 50% MNP content.

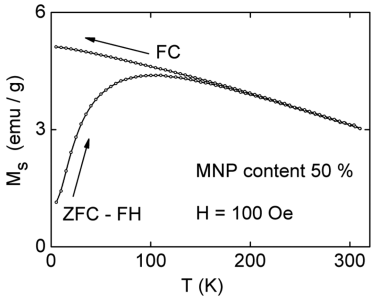

Figure 9. Magnetization of the sample with 50% FF-PAA content as a function of temperature at fixed field (100 Oe). ZFC-FH, zero-field-cooling and field-heating branch; FC, field-cooling branch.

These results are similar to those obtained for other MNP concentrations. The sample was initially cooled in zero field before the measurement. At the lowest temperature, a small, fixed field (100 Oe) larger than the coercive field was applied. Upon heating (lower branch of the curve), the magnetization increased due to thermal activation. Eventually, a crossover temperature was reached, above which paramagnetic-like behavior dominated, indicated by a decrease in the magnetization as the temperature was further increased (T_B, blocking temperature).

In a further step, upon cooling under the magnetic field, the magnetization increased monotonically. These properties are again in good agreement with the assumption that the samples are superparamagnetic.

3.8. Magnetic-Hyperthermia Measurement. Derived from the intrinsic superparamagnetic properties of the MNPs, the gelatin membrane nanocomposites showed excellent hyperthermia properties under exposure to an alternating magnetic field. Figure 10 shows the temperature increase by

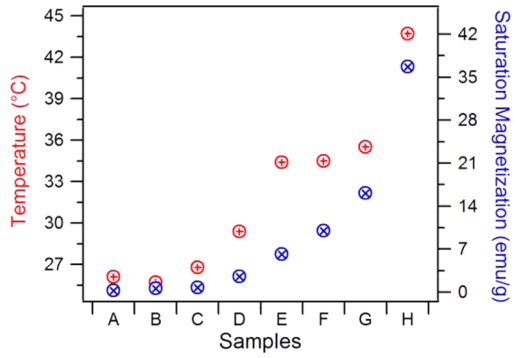

Figure 10. Temperature increase induced in magnetic gelatin membranes by a hyperthermic effect and the magnetization of the membranes. The frequency and intensity of the oscillating magnetic field were 293 kHz and 30 mT, respectively.

hyperthermia when the samples are subjected to an externally applied oscillating magnetic field for 70 s with magnetization of the magnetic gelatin membranes. The hyperthermic effect is evidenced in all samples and increases with the amount of MNPs embedded in the gelatin membranes. Temperature increase up to 43.7 °C were achieved in the magnetic gelatin films with the highest content of magnetic material. These results suggest that by incorporating different amounts of MNPs in the gelatin membranes their magnetic and hyperthermia properties can be tuned. There are different scaffold compositions that have been found to show homogeneous hyperthermia behavior.[66] The assembly of a magnetic gelatin membrane with specific magnetic properties affords not only the formation of magnetic gradients but also the ability to remotely activate temperature gradients inside the 3D biocompatible magnetic scaffolds. These results indicate the possible utilization of such magnetic scaffolds for the triggered and localized release of drugs, growth factors, or other therapeutic agents.

3.9. Magnetic Gradient Simulation. The measured magnetization curves for all membranes were directly included in the modeling process, enabling the best numerical description of the magnetic properties of the scaffolds to be obtained. Two vertical scaffold cases were considered: the first, a homogeneous case, involved seven membranes with the same magnetization (membrane type D), whereas the second, a graded case, involved seven membranes of different magnetization placed in the sequence A, B, C, D, D, D, D and arranged in order of increasing magnetization from bottom to top. In order to bring the modeling as close as possible to real scaffold geometries, the membrane thicknesses were multiplied by a factor of 10 to provide a realistic scaffold thickness of 5.6 mm for both cases. Before moving to detailed COMSOL simulations, we will present estimations of the forces necessary to manipulate the magnetic nanoparticles and the magnetized cells. In general, the force acting on a magnetic dipole of moment $\vec{\mu}$ oriented along the magnetic field $\vec{B}$ is

$$\vec{F} = (\vec{\mu}\cdot\vec{\nabla})\vec{B} \quad (1)$$

where $\vec{\mu}$ is the overall magnetic moment of the MNP and $\vec{B}$ is the magnetic field acting on it.[67] In this study, 9 ± 2 nm diameter superparamagnetic particles with a saturation magnetization of 310 kA/m (60 emu/g) have been used.[68] For superparamagnetic MNPs, the magnetic moment is always oriented along the magnetic field, applied in our calculations

DOI: 10.1021/acsami.5b06813
ACS Appl. Mater. Interfaces 2015, 7, 23098−23109

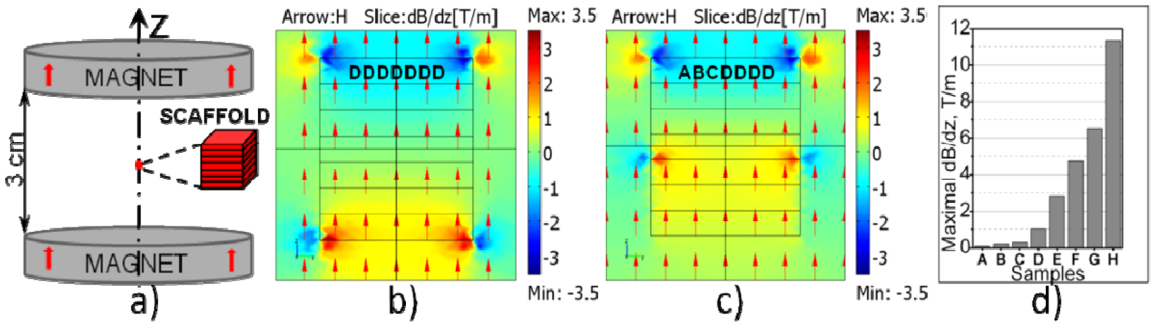

Figure 11. (a) Model geometry. (b, c) Distribution of the gradient of the magnetic induction dB/dz for homogeneous DDDDDDD and graded ABCDDDD stacks cross-sectioned at the xz plane. (d) Maximal magnetic induction gradient dB/dz along the z-axis (perpendicular to the membranes).

along the z-direction (Figure 5). From eq 1, the magnetic force in this case is simply proportional to dB/dz. For magnetically saturated MNPs in an aqueous environment, that is, subject to the Archimedes force, the eq 1 indicates that a magnetic gradient of 0.13 T/m is sufficient to overcome the MNP weight by magnetic attraction. The magnetic manipulation of hMSC cells, due to their relatively high weight, required about 100 pg of MNPs. The whole magnetic moment of this amount is 1.6×10^{-14} Am^2. The weight of a cell (~5 μm diameter) in an aqueous environment can be estimated to be 4.5×10^{-14} N.[69] For a 1.07 g/mL cell density, eq 1 indicates that a 2.7 T/m gradient is necessary to overcome the weight of the cell.[70]

On the basis of the above criteria, the magnetic guiding properties of the stacked DDDDDDD and ABCDDDD scaffolds were investigated by COMSOL finite element analysis. Figure 11a shows the model geometry: multilayered seven-membrane scaffolds, of $5 \times 5 \times 5.6$ mm^3 volume, were placed in the center between two coaxial NdFeB magnet discs (magnetic remanence, B_r = 1.2 T; diameter, 80 mm; height, 10 mm) separated by 30 mm. The red arrows in Figures 11b and 5c indicate that the highly homogeneous magnetic field (H) generated inside the scaffold by the permanent magnets does not influence the total magnetic field gradient.

The calculations evidenced that combining magnetic layers with similar or different magnetizations induces interesting and important modifications of the spatial magnetic induction distribution and hence of the magnetic guiding geometry. Figure 11b shows the magnetic gradient distribution in a stack of seven membranes with the same magnetization corresponding to sample D, whereas Figure 11c presents a stacked scaffold assembled as ABCDDDD membranes with sequentially increasing magnetizations and acceptable biocompatibility (Figure 12). The magnetic field gradients, which are induced in the scaffolds, exceed the background provided by the external magnets, represented by the green color far outside the scaffold and effectively corresponding to zero on the chosen scale in Figure 11b,c. The homogeneous stack DDDDDDD (Figure 11b) shows local gradients exceeding 3 T/m, above the cell-moving and well above the MNP-moving threshold values. The maximum gradients are localized near the surface of the stack, whereas zero gradient (green color) is established in the central part (near z = 0) and represents the region of final cell accumulation and trapping.

Compared to the homogeneous stack, the trapping region in the ABCDDDD scaffold (Figure 11c) was shifted toward the more magnetic layers, keeping it inside the scaffold but closer to the top surface. This is an important finding since by

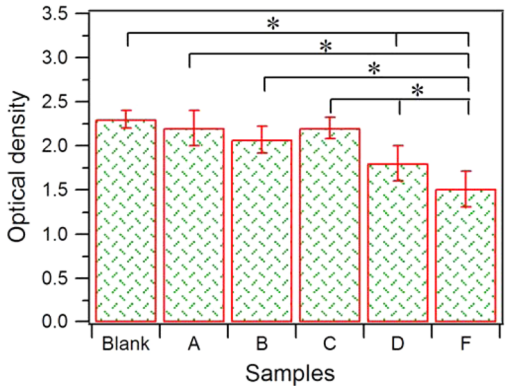

Figure 12. Viability of cells seeded on the surface of magnetized gelatin plates as a function of the concentration of MNPs. Statistical analysis was performed by one-way ANOVA posthoc t-tests, $p < 0.05$, with Bonferroni correction.

assembling magnetic layers, each with the appropriate magnetization, one can accurately select the magnetic trapping region for localized drug delivery or, more generally, for magnetic guiding bioapplications. In both cases, i.e., homogeneous and graded assembling, the calculated gradients were high and sufficient for MNP- and cell-guiding purposes. The use of membranes with higher magnetization provides even higher magnetic gradients and hence more effective guiding (see Figure 11d), but this requires additional work to enhance the biocompatibility of the high-magnetization membranes. These magnetic gradients translate into thermal gradients when the biocompatible scaffolds are subjected to an oscillating magnetic field. The variable magnetic content in the gelatin membranes determines their magnetic hyperthermia performance: the higher the amount of MNPs inside the gelatin nanocomposite film, the higher the saturation magnetization and the temperature increase under an external oscillating magnetic field (Figures 8 and 10). These results are in good agreement with the magnetic induction gradient dB/dz observed along the z-axis (perpendicular to the membranes) in the 3D gelatin membrane stacks by COMSOL finite element analysis (Figure 11d), in which the dB/dz along the z-axis was found to be maximal for the gelatin membrane with the highest concentration of MNPs. Therefore, we will be able to modulate the magnetic and thermal parameters of the final 3D multilayer scaffold by properly assembling individual magnetic gelatin membranes with particular magnetic and hyperthermia properties.

DOI: 10.1021/acsami.5b06813
ACS Appl. Mater. Interfaces 2015, 7, 23098−23109

3.10. Cytotoxicity Analysis. An MTT assay of gelatin and magnetic gelatin membranes A, B, C, D, and F showed that there was no difference in cell viability between samples A, B, and C and the nonmagnetic blank control sample (Figure 12). A loss of viability was observed with sample D, which further decreased as the concentration of MNPs increased. The viability decreased further with increasing magnetization (sample F). These results suggest that the system containing cross-linked gelatin with MNPs (A, B, and C, as well as D to a lesser degree) preserved cell viability. Further research is needed to improve protocols for the biocompatibility of the samples with higher concentrations of MNPs (samples E–H).

A live–dead assay was performed to examine the viability of the cells with increasing concentrations of MNPs compared with that of cells on a control tissue culture plate (TCP). The cells on the membrane scaffolds were examined by fluorescence microscopy after live–dead staining (Figure 13). Two days after seeding the cells, the membrane scaffolds with a lower concentration of MNPs (Figure 13, sample A) resulted in no difference in viability when compared to that of TCP. However, with increasing concentrations of MNPs in the membrane scaffolds (Figure 13, samples D and F), some red spots were observed, representing dead cells.

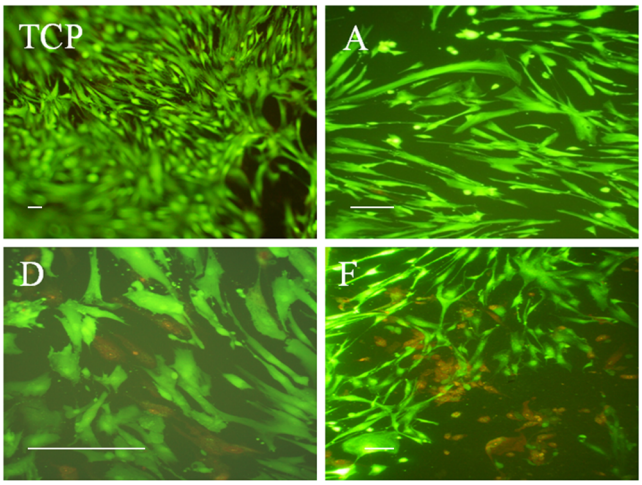

Figure 13. Live–dead assay of hMSCs cultured on magnetized gelatin membranes A (sample A), D (sample D), and F (sample F) compared to that on TCP (tissue culture plate); scale bars, 100 μm.

3.11. Cell Manipulation and Localization under an External Magnetic Field. The viability of magnetized hMSCs after cell manipulation by 1.2 T magnetic field was performed. Three different concentrations of MNPs were chosen for the experiments, and it was observed that the viability of the cells was not affected by any of the concentrations of MNPs compared to the blank sample without any MNPs (Figure 14).

For a proof-of-concept study of the efficiency of cell manipulation by magnetized gelatin, an in vitro experiment was performed in which the vertical geometry of the scaffolds presented in Figure 15 was substituted, for simplicity and optical accessibility, by the planar geometry. The dark part corresponds to the magnetized membrane, and the light part indicates the blank nonmagnetic gelatin. Figure 15a–c shows the cell motility starting from time zero (a), followed by that at 5 min (b) and 20 min (c). The motion of the cells was initiated after a few seconds: Figure 8a shows a random distribution of cells all over the nonmagnetic part (light color), Figure 15b shows a partial accumulation of cells near the magnetic strip, and Figure 15c registers the nearly complete accumulation of magnetized hMSCs near the edge of the C magnetized gelatin.

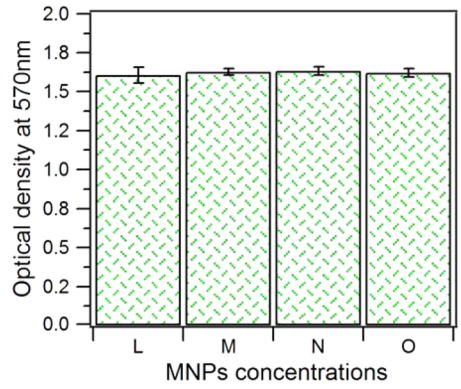

Figure 14. Viability of magnetized hMSCs (L = without any MNPs/cell; M = 50 pg, N = 100 pg, and O = 200 pg MNPs/cell) after cell manipulation by a 1.2 T magnetic field. Statistical analysis was performed by one-way ANOVA; the difference is not significant ($p > 0.05$) between groups. Data are presented as the average; $n = 6$.

The result indicates that magnetic gelatin scaffolds, even at low magnetic concentrations, are able to alter the externally applied magnetic field and create field gradients sufficiently strong to attract magnetized cells. Figure 8d shows the results of COMSOL calculations for this planar geometry. The calculations were performed in a radial symmetry, keeping the magnet in the same plane with its edge at 15 mm from the magnetic strip and approximating the strip by a 3 mm wide ring. One can see that for this configuration strong, sharply localized radial magnetic gradients (dB/dx) exceed the cell-guiding limit of 4 T/m. These gradients are narrowly concentrated at the magnetized gelatin edges, exactly where the cell accumulation was experimentally observed. It is also possible to appreciate an interesting inversion of the gradient from negative (attraction) to positive (repulsion) at the very external edge of the ring. This additional local effect will be investigated in detail in future experiments with higher optical resolution. It is noteworthy that the cells seeded on the surface of magnetized gelatin scaffolds maintained their viability and showed no significant difference in comparison with the control.

4. CONCLUSIONS

The multilayer approach adopted in this study provides a means for fine-tuning magnetic gradients and local magnetic minima that act as trapping centers of magnetized cells. Gelatin is a flexible and adaptable material for such magnetic scaffolds with good biocompatibility, enabling it to be used for in vitro investigations. These membrane scaffolds showed hyperthermic properties under exposure to an alternating magnetic field. These results indicate the possible utilization of such scaffolds for the targeted and triggered release of drugs, growth factors, or other therapeutic agents. The magnetic gelatin scaffolds do not impart significant cytotoxic effects to hMSCs. The results demonstrate that such magnetic scaffolds with tunable magnetic gradients can support the attachment of hMSCs and that they can be positioned using an external magnetic field, which could be useful for tissue engineering applications. Additionally, the tunable hyperthermic properties of the individual gelatin membranes under an oscillating magnetic field open the

DOI: 10.1021/acsami.5b06813
ACS Appl. Mater. Interfaces 2015, 7, 23098–23109

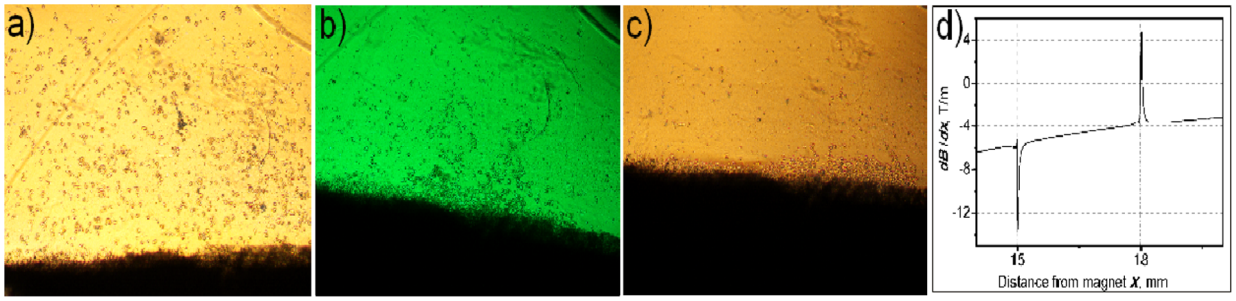

Figure 15. Time distribution of magnetized hMSCs throughout a magnetized gelatin sample under an applied magnetic field. Magnetically labeled cells accumulated on the boarder of the magnetized part of the gelatin surface at (a) 0 min, (b) 5 min, and (c) 20 min under an applied external magnetic field. The magnetic forces were calculated by COMSOL for the experimental configuration and material choice at the edge of the magnetic part, where the (d) gradient has sharp peaks.

possibility of inducing thermal gradients in the multilayer stacks that would enable the triggered release of growth factors and therapeutic compounds along the designed direction inside the scaffold.

AUTHOR INFORMATION

Corresponding Authors

*(D.L.K.) Tel.: +16176270851. Fax: +16176273231. E-mail: david.kaplan@tufts.edu.
*(V.A.D.) E-mail: v.dediu@bo.ismn.cnr.it.

Notes

The authors declare no competing financial interest.

ACKNOWLEDGMENTS

The authors would like to thank the EC-FP7 project MAGISTER (NMP3-LA-2008-214685), the NIH (EB002520), and the AFOSR for financial support. The support of the HLD at HZDR, a member of the European Magnetic Field Laboratory (EMFL), is also acknowledged. The authors also thank Biodevice Systems for the biological experiments.

REFERENCES

(1) Hollister, S. J. Porous Scaffold Design for Tissue Engineering. *Nat. Mater.* **2005**, *4*, 518−524.
(2) Dueber, J. E.; Wu, G. C.; Malmirchegini, G. R.; Moon, T. S.; Petzold, C. J.; Ullal, A. V.; Prather, K. L. J.; Keasling, J. D. Synthetic Protein Scaffolds Provide Modular Control over Metabolic Flux. *Nat. Biotechnol.* **2009**, *27*, 753−U107.
(3) Andersen, M. O.; Nygaard, J. V.; Burns, J. S.; Raarup, M. K.; Nyengaard, J. R.; Bunger, C.; Besenbacher, F.; Howard, K. A.; Kassem, M.; Kjems, J. siRNA Nanoparticle Functionalization of Nanostructured Scaffolds Enables Controlled Multilineage Differentiation of Stem Cells. *Mol. Ther.* **2010**, *18*, 2018−2027.
(4) Bock, N.; Riminucci, A.; Dionigi, C.; Russo, A.; Tampieri, A.; Landi, E.; Goranov, V. A.; Marcacci, M.; Dediu, V. A Novel Route in Bone Tissue Engineering: Magnetic Biomimetic Scaffolds. *Acta Biomater.* **2010**, *6*, 786−796.
(5) Capito, R. M.; Spector, M. Collagen Scaffolds for Nonviral IGF-1 Gene Delivery in Articular Cartilage Tissue Engineering. *Gene Ther.* **2007**, *14*, 721−732.
(6) Schussler, O.; Coirault, C.; Louis-Tisserand, M.; Al-Chare, W.; Oliviero, P.; Menard, C.; Michelot, R.; Bochet, P.; Salomon, D. R.; Chachques, J. C.; Carpentier, A.; Lecarpentier, Y. Use of Arginine-Glycine-Aspartic Acid Adhesion Peptides Coupled with a New Collagen Scaffold to Engineer a Myocardium-Like Tissue Graft. *Nat. Clin. Pract. Cardiovasc. Med.* **2009**, *6*, 240−249.
(7) Kim, J.; Chung, S. E.; Choi, S. E.; Lee, H.; Kim, J.; Kwon, S. Programming Magnetic Anisotropy in Polymeric Microactuators. *Nat. Mater.* **2011**, *10*, 747−752.
(8) Panseri, S.; Cunha, C.; D'Alessandro, T.; Sandri, M.; Russo, A.; Giavaresi, G.; Marcacci, M.; Hung, C. T.; Tampieri, A. Magnetic Hydroxyapatite Bone Substitutes to Enhance Tissue Regeneration: Evaluation in Vitro Using Osteoblast-Like Cells and in Vivo in a Bone Defect. *PLoS One* **2012**, *7*, e38710.
(9) Robert, D.; Fayol, D.; Le Visage, C.; Frasca, G.; Brule, S.; Menager, C.; Gazeau, F.; Letourneur, D.; Wilhelm, C. Magnetic Micro-Manipulations to Probe the Local Physical Properties of Porous Scaffolds and to Confine Stem Cells. *Biomaterials* **2010**, *31*, 1586−1595.
(10) Hu, C. Z.; Uchida, T.; Tercero, C.; Ikeda, S.; Ooe, K.; Fukuda, T.; Arai, F.; Negoro, M.; Kwon, G. Development of Biodegradable Scaffolds Based on Magnetically Guided Assembly of Magnetic Sugar Particles. *J. Biotechnol.* **2012**, *159*, 90−98.
(11) Polyak, B.; Fishbein, I.; Chorny, M.; Alferiev, I.; Williams, D.; Yellen, B.; Friedman, G.; Levy, R. J. High Field Gradient Targeting of Magnetic Nanoparticle-Loaded Endothelial Cells to the Surfaces of Steed Stents. *Proc. Natl. Acad. Sci. U. S. A.* **2008**, *105*, 698−703.
(12) Dames, P.; Gleich, B.; Flemmer, A.; Hajek, K.; Seidl, N.; Wiekhorst, F.; Eberbeck, D.; Bittmann, I.; Bergemann, C.; Weyh, T.; Trahms, L.; Rosenecker, J.; Rudolph, C. Targeted Delivery of Magnetic Aerosol Droplets to the Lung. *Nat. Nanotechnol.* **2007**, *2*, 495−499.
(13) Voros, E.; Cho, M.; Ramirez, M.; Palange, A. L.; De Rosa, E.; Key, J.; Garami, Z.; Lumsden, A. B.; Decuzzi, P. TPA Immobilization on Iron Oxide Nanocubes and Localized Magnetic Hyperthermia Accelerate Blood Clot Lysis. *Adv. Funct. Mater.* **2015**, *25*, 1709−1718.
(14) Dobson, J. Remote Control of Cellular Behaviour with Magnetic Nanoparticles. *Nat. Nanotechnol.* **2008**, *3*, 139−143.
(15) Kolen'ko, Y. V.; Bañobre-López, M.; Rodríguez-Abreu, C.; Carbó-Argibay, E.; Sailsman, A.; Piñeiro-Redondo, Y.; Cerqueira, M. F.; Petrovykh, D. Y.; Kovnir, K.; Lebedev, O. I.; Rivas, J. Large-Scale Synthesis of Colloidal Fe_3O_4 Nanoparticles Exhibiting High Heating Efficiency in Magnetic Hyperthermia. *J. Phys. Chem. C* **2014**, *118*, 8691−8701.
(16) Panseri, S.; Russo, A.; Sartori, M.; Giavaresi, G.; Sandri, M.; Fini, M.; Maltarello, M. C.; Shelyakova, T.; Ortolani, A.; Visani, A.; Dediu, V.; Tampieri, A.; Marcacci, M. Modifying Bone Scaffold Architecture in Vivo with Permanent Magnets to Facilitate Fixation of Magnetic Scaffolds. *Bone* **2013**, *56*, 432−439.
(17) Gloria, A.; Russo, T.; D'Amora, U.; Zeppetelli, S.; D'Alessandro, T.; Sandri, M.; Bañobre-López, M.; Piñeiro-Redondo, Y.; Uhlarz, M.; Tampieri, A.; Rivas, J.; Herrmannsdörfer, T.; Dediu, V. A.; Ambrosio, L.; De Santis, R. Magnetic Poly(E-Caprolactone)/Iron-Doped Hydroxyapatite Nanocomposite Substrates for Advanced Bone Tissue Engineering. *J. R. Soc., Interface* **2013**, *10*.10.1098/rsif.2012.0833
(18) Russo, A.; Shelyakova, T.; Casino, D.; Lopomo, N.; Strazzari, A.; Ortolani, A.; Visani, A.; Dediu, V.; Marcacci, M. A New Approach to Scaffold Fixation by Magnetic Forces: Application to Large

DOI: 10.1021/acsami.5b06813
ACS Appl. Mater. Interfaces 2015, 7, 23098−23109

Osteochondral Defects. *Medical Engineering & Physics* **2012**, *34*, 1287−1293.
(19) Ramalingam, M.; Young, M. F.; Thomas, V.; Sun, L.; Chow, L. C.; Tison, C. K.; Chatterjee, K.; Miles, W. C.; Simon, C. G. Nanofiber Scaffold Gradients for Interfacial Tissue Engineering. *J. Biomater. Appl.* **2013**, *27*, 695−705.
(20) Li, L.; Jiang, W.; Luo, K.; Song, H. M.; Lan, F.; Wu, Y.; Gu, Z. W. Superparamagnetic Iron Oxide Nanoparticles as MRI Contrast Agents for Non-Invasive Stem Cell Labeling and Tracking. *Theranostics* **2013**, *3*, 595−615.
(21) Li, B.; Jia, D.; Zhou, Y.; Hu, Q.; Cai, W. In Situ Hybridization to Chitosan/Magnetite Nanocomposite Induced by the Magnetic Field. *J. Magn. Magn. Mater.* **2006**, *306*, 223−227.
(22) Li, Y.; Huang, G.; Zhang, X.; Li, B.; Chen, Y.; Lu, T.; Lu, T. J.; Xu, F. Magnetic Hydrogels and Their Potential Biomedical Applications. *Adv. Funct. Mater.* **2013**, *23*, 660−672.
(23) Huang, D.-M.; Hsiao, J.-K.; Chen, Y.-C.; Chien, L.-Y.; Yao, M.; Chen, Y.-K.; Ko, B.-S.; Hsu, S.-C.; Tai, L.-A.; Cheng, H.-Y.; Wang, S.-W.; Yang, C.-S.; Chen, Y.-C. The Promotion of Human Mesenchymal Stem Cell Proliferation by Superparamagnetic Iron Oxide Nanoparticles. *Biomaterials* **2009**, *30*, 3645−3651.
(24) Hou, R.; Zhang, G.; Du, G.; Zhan, D.; Cong, Y.; Cheng, Y.; Fu, J. Magnetic Nanohydroxyapatite/PVA Composite Hydrogels for Promoted Osteoblast Adhesion and Proliferation. *Colloids Surf., B* **2013**, *103*, 318−325.
(25) Kim, J.-J.; Singh, R. K.; Seo, S.-J.; Kim, T.-H.; Kim, J.-H.; Lee, E.-J.; Kim, H.-W. Magnetic Scaffolds of Polycaprolactone with Functionalized Magnetite Nanoparticles: Physicochemical, Mechanical, and Biological Properties Effective for Bone Regeneration. *RSC Adv.* **2014**, *4*, 17325−17336.
(26) Dashnyam, K.; Perez, R. A.; Singh, R. K.; Lee, E.-J.; Kim, H.-W. Hybrid Magnetic Scaffolds of Gelatin-Siloxane Incorporated with Magnetite Nanoparticles Effective for Bone Tissue Engineering. *RSC Adv.* **2014**, *4*, 40841−40851.
(27) Tampieri, A.; Iafisco, M.; Sandri, M.; Panseri, S.; Cunha, C.; Sprio, S.; Savini, E.; Uhlarz, M.; Herrmannsdörfer, T. Magnetic Bioinspired Hybrid Nanostructured Collagen−Hydroxyapatite Scaffolds Supporting Cell Proliferation and Tuning Regenerative Process. *ACS Appl. Mater. Interfaces* **2014**, *6*, 15697−15707.
(28) Mack, J. J.; Cox, B. N.; Sudre, O.; Corrin, A. A.; dos Santos e Lucato, S. L.; Ma, C.; Andrew, J. S. Achieving Nutrient Pumping and Strain Stimulus by Magnetic Actuation of Tubular Scaffolds. *Smart Mater. Struct.* **2009**, *18*, 104025.
(29) Markaki, A. E.; Clyne, T. W. Magneto-Mechanical Stimulation of Bone Growth in a Bonded Array of Ferromagnetic Fibres. *Biomaterials* **2004**, *25*, 4805−4815.
(30) Sapir, Y.; Cohen, S.; Friedman, G.; Polyak, B. The Promotion of In Vitro Vessel-Like Organization of Endothelial Cells in Magnetically Responsive Alginate Scaffolds. *Biomaterials* **2012**, *33*, 4100−4109.
(31) Thevenot, J.; Oliveira, H.; Sandre, O.; Lecommandoux, S. Magnetic Responsive Polymer Composite Materials. *Chem. Soc. Rev.* **2013**, *42*, 7099−7116.
(32) Ilg, P. Stimuli-Responsive Hydrogels Cross-Linked by Magnetic Nanoparticles. *Soft Matter* **2013**, *9*, 3465−3468.
(33) Yiu, H. H. P.; Liu, K.-K. Mechanical and Magnetic Stimulation on Cells for Bone Regeneration. In *Biomechanics of Hard Tissues*; Wiley-VCH: Weinheim, Germany, 2010; pp 193−207.
(34) Stock, M.; Kirchner, B.; Waibler, D.; Cowley, D. E.; Pfaffl, M. W.; Kuehn, R. Effect of Magnetic Stimulation on the Gene Expression Profile of in Vitro Cultured Neural Cells. *Neurosci. Lett.* **2012**, *526*, 122−127.
(35) Pashut, T.; Wolfus, S.; Friedman, A.; Lavidor, M.; Bar-Gad, I.; Yeshurun, Y.; Korngreen, A. Mechanisms of Magnetic Stimulation of Central Nervous System Neurons. *PLoS Comput. Biol.* **2011**, *7*, e1002022.
(36) Hellmann, J.; Jüttner, R.; Roth, C.; Bajbouj, M.; Kirste, I.; Heuser, I.; Gertz, K.; Endres, M.; Kronenberg, G. Repetitive Magnetic Stimulation of Human-Derived Neuron-Like Cells Activates cAMP-CREB Pathway. *Eur. Arch. Psychiatry Clin. Neurosci.* **2012**, *262*, 87−91.
(37) Sensenig, R.; Sapir, Y.; MacDonald, C.; Cohen, S.; Polyak, B. Magnetic Nanoparticle-Based Approaches to Locally Target Therapy and Enhance Tissue Regeneration in Vivo. *Nanomedicine* **2012**, *7*, 1425−1442.
(38) Xiong, F.; Chen, Y.; Chen, J.; Yang, B.; Zhang, Y.; Gao, H.; Hua, Z.; Gu, N. Rubik-Like Magnetic Nanoassemblies as an Efficient Drug Multifunctional Carrier for Cancer Theranostics. *J. Controlled Release* **2013**, *172*, 993−1001.
(39) Wang, C.; Ravi, S.; Martinez, G. V.; Chinnasamy, V.; Raulji, P.; Howell, M.; Davis, Y.; Mallela, J.; Seehra, M. S.; Mohapatra, S. Dual-Purpose Magnetic Micelles for MRI and Gene Delivery. *J. Controlled Release* **2012**, *163*, 82−92.
(40) Colomb, J.; Louie, K.; Massia, S. P.; Bennett, K. M. Self-Degrading, MRI-Detectable Hydrogel Sensors with Picomolar Target Sensitivity. *Magn. Reson. Med.* **2010**, *64*, 1792−1799.
(41) Shin, M. K.; Kim, S. I.; Kim, S. J.; Park, S. Y.; Hyun, Y. H.; Lee, Y.; Lee, K. E.; Han, S.-S.; Jang, D.-P.; Kim, Y.-B.; Cho, Z.-H.; So, I.; Spinks, G. M. Controlled Magnetic Nanofiber Hydrogels by Clustering Ferritin. *Langmuir* **2008**, *24*, 12107−12111.
(42) Zhang, Y.; Sun, Y.; Yang, X.; Hilborn, J.; Heerschap, A.; Ossipov, D. A. Injectable in Situ Forming Hybrid Iron Oxide-Hyaluronic Acid Hydrogel for Magnetic Resonance Imaging and Drug Delivery. *Macromol. Biosci.* **2014**, *14*, 1249−1259.
(43) Lee, Y.-C.; Gajdosik, M.; Josic, D.; Lin, S.-H. Plasma Membrane Isolation Using Immobilized Concanavalin a Magnetic Beads. In *Liver Proteomics*; Josic, D., Hixson, D. C., Eds.; Humana Press: New York, 2012; Chapter 3, pp 29−41.
(44) Madaeni, S. S.; Enayati, E.; Vatanpour, V. Separation of Nitrogen and Oxygen Gases by Polymeric Membrane Embedded with Magnetic Nano-Particle. *Polym. Adv. Technol.* **2011**, *22*, 2556−2563.
(45) Meenach, S. A.; Hilt, J. Z.; Anderson, K. W. Poly(ethylene glycol)-Based Magnetic Hydrogel Nanocomposites for Hyperthermia Cancer Therapy. *Acta Biomater.* **2010**, *6*, 1039−1046.
(46) Lin, T.-C.; Lin, F.-H.; Lin, J.-C. In Vitro Feasibility Study of the Use of a Magnetic Electrospun Chitosan Nanofiber Composite for Hyperthermia Treatment of Tumor Cells. *Acta Biomater.* **2012**, *8*, 2704−2711.
(47) Konat Zorzi, G.; Contreras-Ruiz, L.; Párraga, J. E.; López-García, A.; Romero Bello, R.; Diebold, Y.; Seijo, B.; Sánchez, A. Expression of MUC5AC in Ocular Surface Epithelial Cells Using Cationized Gelatin Nanoparticles. *Mol. Pharmaceutics* **2011**, *8*, 1783−1788.
(48) Hiwale, P.; Lampis, S.; Conti, G.; Caddeo, C.; Murgia, S.; Fadda, A. M.; Monduzzi, M. In Vitro Release of Lysozyme from Gelatin Microspheres: Effect of Cross-Linking Agents and Thermoreversible Gel as Suspending Medium. *Biomacromolecules* **2011**, *12*, 3186−3193.
(49) Samal, S. K.; Dash, M.; Van Vlierberghe, S.; Kaplan, D. L.; Chiellini, E.; van Blitterswijk, C.; Moroni, L.; Dubruel, P. Cationic Polymers and Their Therapeutic Potential. *Chem. Soc. Rev.* **2012**, *41*, 7147−7194.
(50) Won, Y.-W.; Yoon, S.-M.; Sonn, C. H.; Lee, K.-M.; Kim, Y.-H. Nano Self-Assembly of Recombinant Human Gelatin Conjugated with α-Tocopheryl Succinate for Hsp90 Inhibitor, 17-AAG, Delivery. *ACS Nano* **2011**, *5*, 3839−3848.
(51) Li, C. Y.; Yuan, W.; Jiang, H.; Li, J. S.; Xu, F. J.; Yang, W. T.; Ma, J. PCL Film Surfaces Conjugated with P(DMAEMA)/Gelatin Complexes for Improving Cell Immobilization and Gene Transfection. *Bioconjugate Chem.* **2011**, *22*, 1842−1851.
(52) Zwiorek, K.; Bourquin, C.; Battiany, J.; Winter, G.; Endres, S.; Hartmann, G.; Coester, C. Delivery by Cationic Gelatin Nanoparticles Strongly Increases the Immunostimulatory Effects of CpG Oligonucleotides. *Pharm. Res.* **2008**, *25*, 551−562.
(53) Piñeiro-Redondo, Y.; Bañobre-López, M.; Pardiñas-Blanco, I.; Goya, G.; López-Quintela, M. A.; Rivas, J. The Influence of Colloidal Parameters on the Specific Power Absorption of PAA-Coated Magnetite Nanoparticles. *Nanoscale Res. Lett.* **2011**, *6*, 383.
(54) Staroszczyk, H.; Sztuka, K.; Wolska, J.; Wojtasz-Pająk, A.; Kołodziejska, I. Interactions of Fish Gelatin and Chitosan in Uncrosslinked and Crosslinked with EDC Films: FT-IR Study. *Spectrochim. Acta, Part A* **2014**, *117*, 707−712.

DOI: 10.1021/acsami.5b06813
ACS Appl. Mater. Interfaces 2015, 7, 23098−23109

(55) Chang, J.-Y.; Lin, J.-H.; Yao, C.-H.; Chen, J.-H.; Lai, T.-Y.; Chen, Y.-S. In Vivo Evaluation of a Biodegradable EDC/NHS-Cross-Linked Gelatin Peripheral Nerve Guide Conduit Material. *Macromol. Biosci.* **2007**, *7*, 500−507.
(56) Kuijpers, A. J.; Engbers, G. H. M.; Krijgsveld, J.; Zaat, S. A. J.; Dankert, J.; Feijen, J. Cross-Linking and Characterisation of Gelatin Matrices for Biomedical Applications. *J. Biomater. Sci., Polym. Ed.* **2000**, *11*, 225−243.
(57) Cammarata, C. R.; Hughes, M. E.; Ofner, C. M. Carbodiimide Induced Cross-Linking, Ligand Addition, and Degradation in Gelatin. *Mol. Pharmaceutics* **2015**, *12*, 783−793.
(58) Bartholomew, A.; Sturgeon, C.; Siatskas, M.; Ferrer, K.; McIntosh, K.; Patil, S.; Hardy, W.; Devine, S.; Ucker, D.; Deans, R.; Moseley, A.; Hoffman, R. Mesenchymal Stem Cells Suppress Lymphocyte Proliferation in Vitro and Prolong Skin Graft Survival in Vivo. *Exp. Hematol.* **2002**, *30*, 42−48.
(59) Mosmann, T. Rapid Colorimetric Assay for Cellular Growth and Survival: Application to Proliferation and Cytotoxicity Assays. *J. Immunol. Methods* **1983**, *65*, 55−63.
(60) García, R.; Pérez, R. Dynamic Atomic Force Microscopy Methods. *Surf. Sci. Rep.* **2002**, *47*, 197−301.
(61) Kiely, J. D.; Bonnell, D. A. Quantification of Topographic Structure by Scanning Probe Microscopy. *J. Vac. Sci. Technol., B: Microelectron. Process. Phenom.* **1997**, *15*, 1483−1493.
(62) Ramdani, A.; Steinmetz, J.; Gleitzer, C.; Coey, J. M. D.; Friedt, J. M. Perturbation De L'echange Electronique Rapide Par Les Lacunes Cationiques Dans $Fe_{3-x}O_4$ ($x \leqslant 0{,}09$). *J. Phys. Chem. Solids* **1987**, *48*, 217−228.
(63) Kim, D. K.; Zhang, Y.; Voit, W.; Rao, K. V.; Muhammed, M. Synthesis and Characterization of Surfactant-Coated Superparamagnetic Monodispersed Iron Oxide Nanoparticles. *J. Magn. Magn. Mater.* **2001**, *225*, 30−36.
(64) Kaiser, R.; Miskolczy, G. Magnetic Properties of Stable Dispersions of Subdomain Magnetite Particles. *J. Appl. Phys.* **1970**, *41*, 1064−1072.
(65) Samal, S. K.; Dash, M.; Shelyakova, T.; Declercq, H. A.; Uhlarz, M.; Bañobre-López, M.; Dubruel, P.; Cornelissen, M.; Herrmannsdörfer, T.; Rivas, J.; Padeletti, G.; De Smedt, S.; Braeckmans, K.; Kaplan, D. L.; Dediu, V. A. Biomimetic Magnetic Silk Scaffolds. *ACS Appl. Mater. Interfaces* **2015**, *7*, 6282−6292.
(66) Banobre-Lopez, M.; Pineiro-Redondo, Y.; Sandri, M.; Tampieri, A.; De Santis, R.; Dediu, V. A.; Rivas, J. Hyperthermia Induced in Magnetic Scaffolds for Bone Tissue Engineering. *IEEE Trans. Magn.* **2014**, *50*, 1−7.
(67) Furlani, E. P. Analysis of Particle Transport in a Magnetophoretic Microsystem. *J. Appl. Phys.* **2006**, *99*, 024912−11.
(68) Goya, G. F.; Berquo, T. S.; Fonseca, F. C.; Morales, M. P. Static and Dynamic Magnetic Properties of Spherical Magnetite Nanoparticles. *J. Appl. Phys.* **2003**, *94*, 3520−3528.
(69) Castromalaspina, H.; Gay, R. E.; Resnick, G.; Kapoor, N.; Meyers, P.; Chiarieri, D.; Mckenzie, S.; Broxmeyer, H. E.; Moore, M. A. S. Characterization of Human-Bone Marrow Fibroblast Colony-Forming Cells (CFU-F) and Their Progeny. *Blood* **1980**, *56*, 289−301.
(70) Bhartiya, D.; Shaikh, A.; Nagvenkar, P.; Kasiviswanathan, S.; Pethe, P.; Pawani, H.; Mohanty, S.; Rao, S. G. A.; Zaveri, K.; Hinduja, I. Very Small Embryonic-Like Stem Cells with Maximum Regenerative Potential Get Discarded During Cord Blood Banking and Bone Marrow Processing for Autologous Stem Cell Therapy. *Stem Cells Dev.* **2012**, *21*, 1−6.

DOI: 10.1021/acsami.5b06813
ACS Appl. Mater. Interfaces 2015, 7, 23098−23109